

# POSTBUCKLING ANALYSIS AND OPTIMIZATION OF STIFFENED FUSELAGE PANELS UTILIZING VARIABLE-STIFFNESS LAMINATES

**Tanut Ungwattanapanit, Horst Baier**  
**Technische Universitaet Muenchen, Germany**

**Keywords:** *post-buckling, curvilinear fibers, optimization, stiffened fuselage side panels*

## Abstract

*The optimization of a composite stiffened fuselage window belt made by steered-fiber laminates subject to a torsional moment demonstrates 26% post-buckling stability improvement compared to a conventional straight-fiber design. The nonlinear buckling stability is evaluated by maximum skin's transverse displacement in this research work. Post-optimization evaluations reveal that the optimal panel has 23% lower Tsai-Wu failure index and 10% reduction in in-plane shear stiffness compared to the reference design. The investigation paves a way towards significant airframe weight saving by utilizing curvilinear fibers. In order to avoid local optimum traps, Global Response Surface Method (GRSM) is selected as a more efficient optimization procedure compared to conventional evolutionary algorithms. Implicit nonlinear finite element solver Abaqus is utilized to produce nonlinear geometrical responses.*

## 1 Introduction

Superior buckling stability obtained by steered-fiber laminates [1],[2],[3] has, in recent years, widely attracted interests from aerospace research community whose ultimate goal is radical reduction in vehicle fuel consumption.

Since buckling stability is undoubtedly one of the most important aspects in thin-walled structure designs, considerable mass reduction is expected if buckling performance is largely improved. Illustrated in Figure 1, structural performance in post-buckling regime is nowadays largely unexploited. Allowing limit load to be significantly higher than first

buckling critical load and permitting onset of composite material degradation between limit load and ultimate load would likely lead to substantial structural mass saving, and consequently low fuel consumption.

Shown in Figure 2, a composite stiffened side panel containing window cutout of a narrow-body airliner model developed in-house was studied. Since presence of cutouts in thin-walled structures makes not only buckling a critical structural aspect, but also high stress concentration around the cutouts, steered-fibers laminates were proposed by authors in this research to mitigate these problems without having to sacrifice by adding more reinforcing material.

## 2 Variable-Stiffness Laminates

### 2.1 Linearly Varied Fiber Paths

Coined by Z. Gürdal and R. Olmedo [4], linearly varied fiber path provides an in-plane curvilinear fiber path by only two control points (or fiber angles) at the plate center and plate edge respectively. Thanks to its ability to beneficially distribute in-plane buckling loads towards stiff edges where boundary conditions or stiffeners are put in place, 35-67% compressive buckling load improvement has been demonstrated by using linearly varied fiber path compared to straight-fiber laminates [5]. Nonlinearly varied fiber paths would further increase the buckling resistance. The constitutive equation of linearly varied fiber path along y-axis of a rectangular flat plate is the following:

$$\theta(y) = T_0 + \frac{2|y|}{b} (T_1 - T_0) \quad (1)$$

where

- $T_0$  = input fiber orientation at  $y=0$
- $T_1$  = input fiber orientation at  $y=\pm b/2$
- $b$  = plate's length in  $y$ -axis
- $\theta(y)$  = subsequent fiber orientation at  $0 < y < b/2$  and  $-b/2 < y < 0$

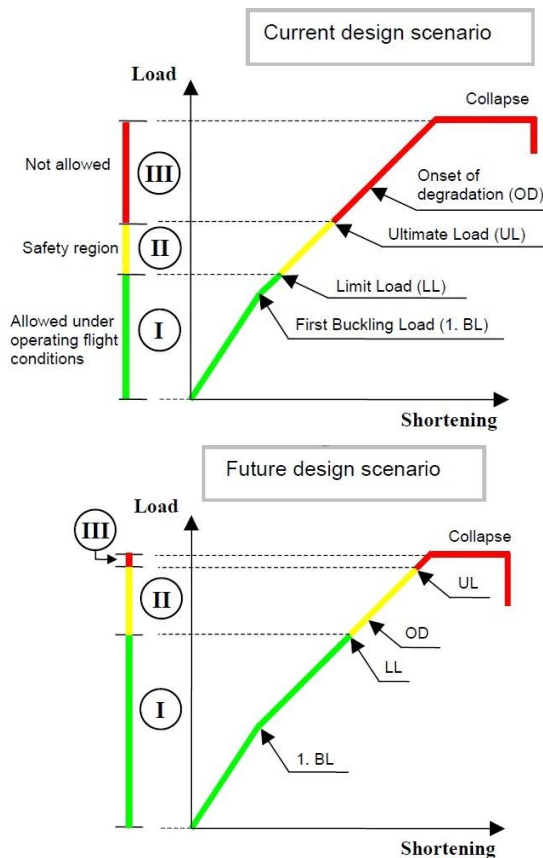


Figure 1 Current & future design scenarios under buckling load [6]



Figure 2 TUM-LLB Flieger fuselage model

Corresponding linearly varied fiber path can be illustrated in Figure 3.

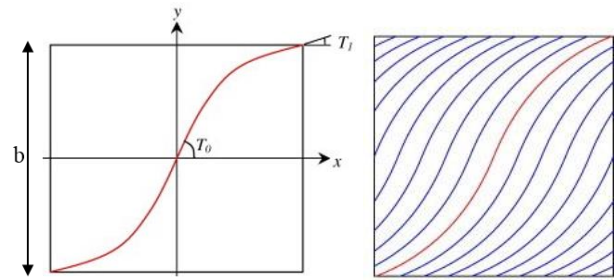


Figure 3 Linearly varied fiber pattern (left);  $\langle 60|15 \rangle$  fiber path with variation along  $y$ -axis (right) [7]

In order to model curvilinear fiber path inside a finite element model, the panel was spatially discretized into 24 sets of finite elements along  $y$ -axis, as shown in Figure 4. Fiber angle variation was linearly varied from angle  $\alpha_1$  at the panel center to angle  $\alpha_2$  at the boundary where the thick skin ended, and from angle  $\alpha_2$  to angle  $\alpha_3$  at the panel edges. Fiber orientation in every finite element belonging to the same set was identical. Discretization with smaller intervals would lead to more accurate results and higher structural improvement at the cost of model complexity.

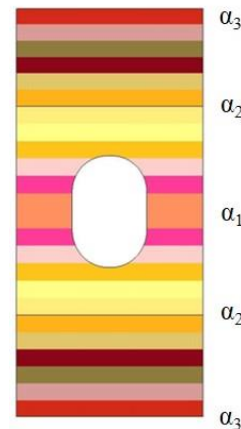
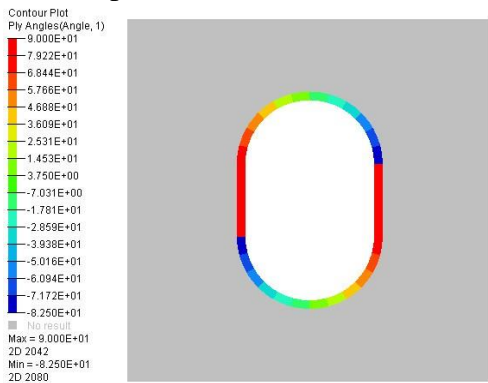


Figure 4 Finite element model discretization for linearly varied fiber path and control angles

## 2.2 Circular Fiber Path

Inspired by research works conducted by M. Hyer et al [8],[9], further investigations [10],[11] showed that aligning fibers around circular or elongated holes, as shown in Figure

5, extensively reduced stress peaks at the cutouts edge when tensile, or to a lesser extent, when shear loads are applied. Adding circular fiber layers C with a quasi-isotropic laminate e.g.  $[\pm 45/90/0/C_4]_s$  increases laminate's in-plane stiffness. On the other hand, this type of laminate is rather unfavorable to buckling resistance, it is therefore recommended to place the circular fiber layers at only proximity from cutout edges. Although not optimized, the circular fiber laminate  $[\pm 45/90/0/C_4]_s$  can be chosen as a predefined stress peak reducer at cutouts without being undergone design optimization process.



**Figure 5 Circular fiber pattern around cabin window cutout (elongated hole)**

Similar finite element grouping technic to linearly varied fiber pattern was applied to the circular fiber course.

### 3 Nonlinear Post-buckling Optimization

In this research work, nonlinear post-buckling optimization was conducted to obtain optimal variable-stiffness fuselage panel for post-buckling stability represented by maximum transverse displacement. The optimal design obtained was then compared against conventional baseline and the best straight-fiber designs. Maximum first-ply failure index and in-plane shear stiffness were also evaluated and compared.

#### 3.1 Optimization by Global Response Surface Method (GRSM)

##### 3.1.1 Optimization Procedure

Suitable for nonconvex design optimization problems where system responses are computationally expensive, GRSM is capable of obtaining global or close-to-global optimal solution with relatively small number of system evaluations [20]. Its efficiency and accuracy come from balanced local-global search capability. Local solutions are found from gradient-based optimization of adaptive surrogate. Global solutions are found from exploratory optimization algorithm. Illustrated in Figure 6, its optimization process starts with response surface constructed by certain number of initial sample points. After the first iteration, the response surface based optimization generates a few designs globally and locally to ensure balanced search capability. Response surface is adaptively updated in every iteration, leading to more accurate approximation. The algorithm finds the local solution on this adaptive surface. In parallel, global sampling is executed to avoid local optima. The best designs from previous iterations are used to generate a new response surface in the next iteration. GRSM will terminate if either maximum number of model evaluation is reached, or the combination of two criteria: minimum number of model evaluation is exceeded and normalized distance between the newly generated design and any of existing designs is less than convergence criteria value specified by user is fulfilled. Efficiency can also be gained by parallel computing as design evaluations are completely independent. GRSM is readily available inside a solver-neutral, commercial optimizer HyperStudy [18],[19].

Verifying optimal solution obtained by GRSM against that from genetic algorithm (GA) revealed identical optimal design in case of straight-fiber design. Though not exactly identical, highly agreeable solutions, with less than 2% difference, obtained from GRSM and GA were observed in the case of variable stiffness design. Please note that these optimization algorithm verifications are not presented in details in this paper.

GRSM parameters specified in HyperStudy for this research are the following:

Maximum Evaluations: 500  
 Minimum Evaluations: 25  
 Initial Sample Points: 50  
 Parallel Processed Designs: 5  
 Convergence Criteria: 0.005  
 With the initial sample points of 11 (no. of design variables+2) being the default value, the GRSM's max. initial sample points of 50 was conservatively chosen. Verification against genetic algorithm's optimum confirmed validity of the chosen GRSM parameters.

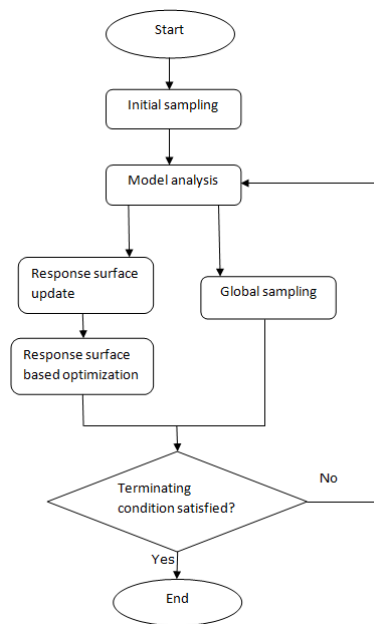


**Figure 6 Global Response Surface Method flow chart [18]**

**3.1.2 Optimization Problem Formulation**

For the considered design optimization problem the design objective was to minimize the maximum transverse displacement  $w_{max}$  of panel skin under torsion by varying control fiber angles  $\mathbf{x}$ . As stress peak reduction was expected by the use of curvilinear fibers around the cutout, it was decided not to include strength constraints, i.e. max. failure index of a conventional design, in the optimization formulation in order to save the already high computational cost. Several quantities, i.e. max. failure index, min. radius of fiber curvature, torsional stiffness, were however later evaluated and compared to those of baseline design. The optimization problem is formulated as:

$$\min w_{max}(\mathbf{x})$$

subject to  $0^\circ \leq \mathbf{x} \leq 90^\circ$

where

in case of constant-stiffness design,

$$\mathbf{x}_{CS} = \{D, E, F, G\} \tag{2}$$

in case of variable-stiffness design,

$$\mathbf{x}_{VS} = \{\alpha_1, \alpha_2, \alpha_3, \beta_1, \beta_2, \beta_3, \gamma_1, \gamma_2, \gamma_3\} \tag{3}$$

The three control angles for each of three layers are design variables in variable-stiffness skin. As for the straight-fiber panel, only single control angle is required per layer. The additional angle, G, is fiber orientation at window frame. The corresponding laminate stacking sequences for both conventional and curvilinear design are described in the next chapter.

**3.2 Post-buckling Analysis**

**3.2.1 Finite element selection**

Two-dimensional shell elements S4R and S3R with sufficiently fine mesh were proven to efficiently provide accurate nonlinear buckling behavior of stiffened plates under compression or shear load [12],[13]. These types of elements were therefore utilized in this research while 10-mm element size was found to be optimal for such type of analysis.

**3.2.2 Structural Idealization**

Adhesive connecting skin to stringers and to window frame was idealized to be rigid elements (KINCOUP). In reality, adhesive layer is expected to fail first and debonding between components is considered critical to fuselage panel subject to buckling loads. Nevertheless, at relatively low load magnitude perfect bonding assumption remains valid.

**3.2.3 Material Properties**

Orthotropic lamina properties were assumed. Referred Carbon-Epoxy IM8/E8552 prepreg properties are tabulated in Table 1. The chosen material has been used in real commercial aircraft fuselages. Material nonlinearity was however neglected based on an assumption of linear material behavior of multi-layered carbon composites even at slightly higher load than first-ply-failure (FPF) load. Maximum Tsai-Wu failure index was 1.68, approximately equal to 130% FPF load in our case.

Material strengths of circular fiber layers were reduced by 14% to take non-continuous fibers' strengths potentially manufactured by Fiber Patch Preforming (FPP) technic [14] into account. E-moduli remained identical to original properties.

E11 [MPa]	157000
E22 [MPa]	12000
$\nu_{12}$ [-]	0.32
G12, G13, G23 [MPa]	5929
S1T [MPa]	2724
S1C [MPa]	1690
S2T [MPa]	64
S2C [MPa]	286
S12 [MPa]	120
S23 [MPa]	137

**Table 1 CFRP IM8/E8552 material properties [15],[16]**

Tsai-Wu first-ply failure criterion was chosen. Failure indices were calculated by the following equation:

$$\begin{aligned}
 FI &= \sigma_1 \left[ \frac{1}{S_{1T}} - \frac{1}{S_{1C}} \right] + \sigma_2 \left[ \frac{1}{S_{2T}} - \frac{1}{S_{2C}} \right] + \frac{\sigma_1^2}{S_{1T}S_{1C}} \\
 &+ \frac{\sigma_2^2}{S_{2T}S_{2C}} + 2F_{12}\sigma_1\sigma_2 + \left( \frac{\tau_{12}}{S_{12}} \right)^2
 \end{aligned} \quad (4)$$

Bi-axial interaction term  $F_{12}$  was assumed to be:

$$F_{12} = -0.5 \sqrt{\left( \frac{1}{S_{1T}S_{1C}S_{2T}S_{2C}} \right)} \quad (5)$$

### 3.2.4 Load & Boundary Conditions

Concentrated torsional moment of  $5.816 \times 10^8$  Nmm, the amount equivalent to twice the critical eigen buckling load of the reference design, was applied at the cylindrical panels' center. Torsional moment producing in-plane shear stress is one of the most critical design loads of fuselage side panels. Sources of in-plane shear stress in real aircraft operations however include not only torsion generated by a lateral force at rudder but also a vertical shear force generated by elevators. Rigid beam elements (COUP\_KIN) then transferred the torsion into in-plane shear displacement load at

the panel's curved edge as depicted in Figure 7. All four edges were clamped to represent stringers and frames.

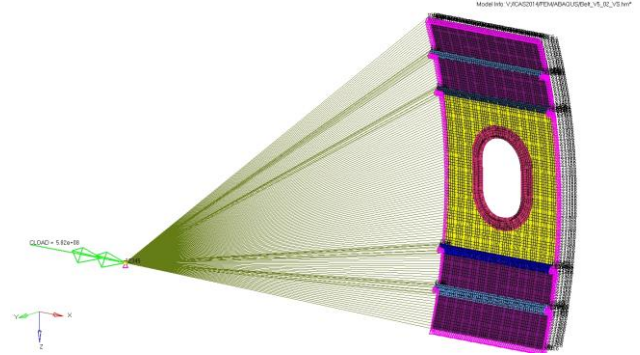


**Figure 7 Torsional moment application in finite element model**

### 3.2.5 Solution Procedure

In this investigation, geometrical nonlinearity caused by torsional moment was simulated. Implicit nonlinear finite element solver Abaqus Standard was employed. Adaptive automatic damping algorithm embedded in Newton's method (\*STATIC, STABILIZE [17]) with default value  $2 \times 10^{-4}$  of the dissipated energy fraction was chosen over Riks method due to superior convergence rate and computational stability. Geometrical imperfection was not considered in this research.

## 4 Model Description

### 4.1 Panel Geometry

Depicted in Figure 7, a cylindrical fuselage panel of a single-aisle airliner model TUM-LLB Flieger (see Figure 2) was investigated. Only the stiffened side panel containing window cutout between two fuselage frames was studied. The geometrical data of this fuselage window belt is tabulated in Table 2.

The J-stringers were initially of extruded aluminum design, but were directly replaced with composite laminates so as to have pure composite fuselage panels in this study.

## 4.2 Stacking Sequences

There were three different designs: reference, constant-stiffness, and variable-stiffness, which were studied in this research. All three panel geometries were identical, while laminate definition being the only difference. Ply thickness was always set to 0.125mm regardless of laminate type.

Radius [mm]	1975
Arc length [mm]	1301
Frame pitch [mm]	587
Stringer cross section	
Stringer pitch [mm]	656 / 164
Stringer thickness [mm]	2.5
Skin thickness [mm]	3.0 / 2.0
Window radius [mm]	105
Window length [mm]	324
Window frame cross section	
Window horizontal frame thickness [mm]	2.0
Window vertical frame thickness [mm]	3.75

**Table 2 Panel geometrical data**

### 4.2.1 Reference Design (REF)

Containing only conventional fiber angles of +45°, -45°, 0°, and 90°, the reference design served as a baseline to be compared with. Its stacking sequences are specified in Table 3.

Component	Stacking Sequence
Skin with cutout	[+45/-45/0/90] <sub>3S</sub>
Skin without cutout	[+45/-45/0/90] <sub>2S</sub>
Window horizontal frame	[+45/-45/0/90] <sub>2S</sub>
Window vertical frame	[+45/-45/0] <sub>5S</sub>
Stringer	[0/90/+45/-45/0/90/-45/+45/90/0] <sub>S</sub>

**Table 3 Reference design's laminate stacking sequences**

### 4.2.2 Constant-Stiffness Design (CS)

Optimal straight-fiber laminates were searched for in order to demonstrate structural performance gained by the best constant-stiffness panel. Its stacking sequences are specified in Table 4. Design variables from (4) are included.

Component	Stacking Sequence
Skin with cutout	[±D/±E/±F] <sub>2S</sub>
Skin without cutout	[±D/±E/±F/+45/-45] <sub>S</sub>
Window horizontal frame, inner	[+45/-45/0/90/±G/±G] <sub>S</sub>
Window horizontal frame, outer	[0/90/±G/±G/±G] <sub>S</sub>
Window vertical frame	[+45/-45/0] <sub>5S</sub>
Stringer	[0/90/+45/-45/0/90/-45/+45/90/0] <sub>S</sub>

**Table 4 Constant-stiffness design's laminate stacking sequences**

### 4.2.3 Variable-Stiffness Design (VSY)

Optimal steered-fiber laminates were searched for in order to demonstrate structural performance gained by variable-stiffness panel; variation was along y-axis in this case. Its stacking sequences are specified in Table 5. Design variables from (5) and circular fiber pattern, C, are included.

Component	Stacking Sequence
Skin with cutout	[±<α <sub>1</sub>  α <sub>2</sub>  α <sub>3</sub> >/±<β <sub>1</sub>  β <sub>2</sub>  β <sub>3</sub> >/±<γ <sub>1</sub>  γ <sub>2</sub>  γ <sub>3</sub> >] <sub>2S</sub>
Skin without cutout	[±<α <sub>1</sub>  α <sub>2</sub>  α <sub>3</sub> >/±<β <sub>1</sub>  β <sub>2</sub>  β <sub>3</sub> >/±<γ <sub>1</sub>  γ <sub>2</sub>  γ <sub>3</sub> >/+45/-45] <sub>S</sub>
Window horizontal frame, inner	[+45/-45/0/90/C <sub>4</sub> ] <sub>S</sub>
Window horizontal frame, outer	[0/90/C <sub>6</sub> ] <sub>S</sub>
Window vertical frame	[+45/-45/0] <sub>5S</sub>
Stringer	[0/90/+45/-45/0/90/-45/+45/90/0] <sub>S</sub>

**Table 5 Variable-stiffness design's laminate stacking sequences**

## 5 Results and Discussions

### 5.1 Optimization Results

#### 5.1.1 Constant-Stiffness Design (CS)

Shown in Figure 8, GRSM took 32 iterations to reach a minimal max. transverse displacement of 5.54mm. The total number of evaluations were 181; 7hr. 31min., on an Intel Xeon X5550@2.67GHz Dual CPU, Windows 7 system, was taken to complete the optimization run. The following optimal fiber angles were found: D=90°, E=0°, F=0°, G=33°.

Since the optimal design objective was determined using a surrogate model, a direct finite element analysis was conducted and 5.36-mm transverse displacement was found according to optimal fiber angles obtained.

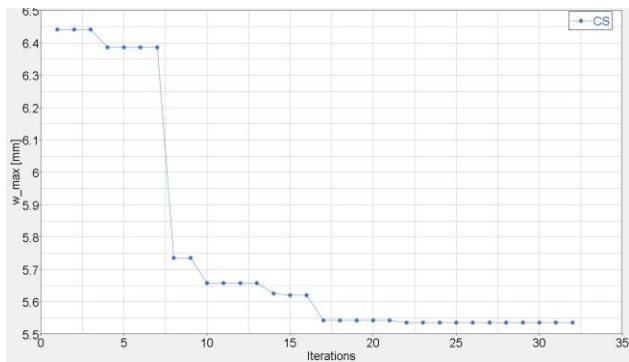


**Figure 8 Optimization history: Max. transverse displacement VS Design iterations of the constant-stiffness design**

#### 5.1.2 Variable-Stiffness Design (VSY)

Shown in Figure 9, GRSM took 44 iterations to reach a minimal max. transverse displacement of 5.4mm. The total number of evaluations were 266; 17hr. 30min., on an Intel Xeon X5550@2.67GHz Dual CPU, Windows 7 system, was taken to complete the optimization run. The following optimal fiber angles were found:

$$\begin{aligned} \langle \alpha_1 | \alpha_2 | \alpha_3 \rangle &= \langle 80 | 90 | 25 \rangle \\ \langle \beta_1 | \beta_2 | \beta_3 \rangle &= \langle 90 | 31 | 28 \rangle \\ \langle \gamma_1 | \gamma_2 | \gamma_3 \rangle &= \langle 2 | 1 | 47 \rangle \end{aligned}$$

Since the optimal design objective was determined using a surrogate model, a direct finite element analysis was conducted and 5.3-

mm transverse displacement was found according to optimal fiber angles obtained.

It was observed that the optimal variable-stiffness laminate favorably distributed in-plane shear loads from weak cutout to stiff edges so that buckles were delayed to a greater load level. For example, optimal fiber orientations at the skin's first layer are shown in Figure 10.

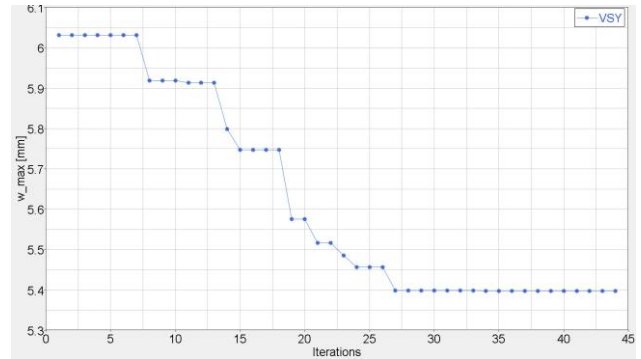


**Figure 9 Optimization history: Max. transverse displacement VS Design iterations of the variable-stiffness design**

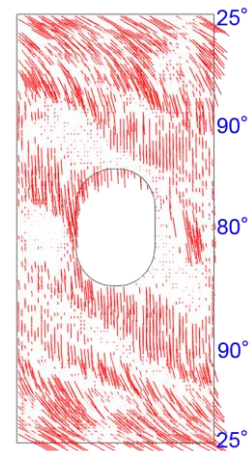


**Figure 10 Optimal linearly varied fiber orientations at skin's 1<sup>st</sup> ply**

### 5.2 Performance Comparison

Optimal variable-stiffness, optimal constant-stiffness, and reference designs were undergone implicit nonlinear analysis. Their structural responses, i.e. max. transverse displacement  $w_{max}$ , failure index FI, circumferential deformation  $u_{max}$ , at 50%, 75%, and 100% load were compared against each other, as shown in Table 6.

2x Limit Load [1.0M <sub>max</sub> ]	Reference Design	Constant-Stiffness Design		Variable-Stiffness Design	
			Improvement [%]		Improvement [%]
Wmax [mm]	7.17	5.36	+25	5.30	+26
FI [-]	1.56	1.68	-8	1.21	+23
Umax [mm]	4.26	7.00	-64	4.68	-10

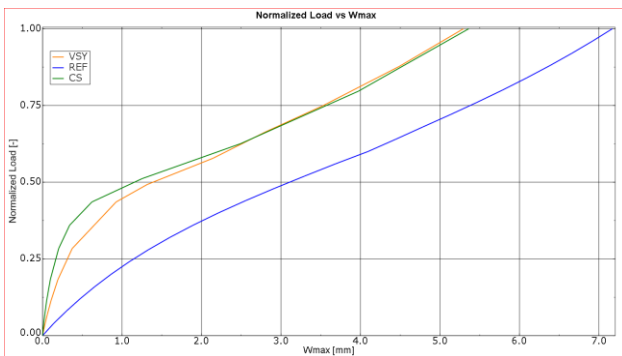
Ultimate Load [0.75M <sub>max</sub> ]	Reference	Constant Stiffness		Variable Stiffness	
			Improvement [%]		Improvement [%]
Wmax [mm]	5.47	3.75	+31	4.10	+25
FI [-]	1.10	1.19	-8	0.91	+17
Umax [mm]	2.95	5.06	-71	3.27	-11

Limit Load [0.5M <sub>max</sub> ]	Reference	Constant Stiffness		Variable Stiffness	
			Improvement [%]		Improvement [%]
Wmax [mm]	3.17	2.23	+30	2.27	+28
FI [-]	0.66	0.76	-16	0.58	+11
Umax [mm]	1.78	3.23	-81	1.95	-10

**Table 6 Post-buckling performance comparison**

Substantiated by Figure 11 and Figure 12, at 100% load where the optimization took place, VSY design improved post-buckling stability by 26% compared to the REF design. Both pre and post-buckling stability improvement can be observed by the VSY design, despite running the optimization at 100% load level alone. CS and VSY designs provided almost identical gain in the post-buckling regime. In terms of stress peak, Max. FI of VSY design was 23% lower than that of REF design, while CS design adversely affected stress concentration at the cutout. This finding confirms the importance of applying curvilinear fibers at window frame in order to simultaneously reduce stress peak while skin stability is being maximized. Failing to alleviate stress raiser will make obtainable stability improvement useless if mass saving or higher load capability is ultimately aimed for.



**Figure 11 Torsional moment VS Transverse displacement plot at the most critical skin position around the cutout (see Figure 12)**

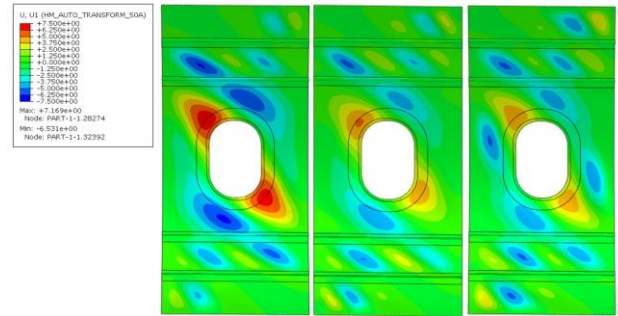


**Figure 12 Transverse deformation fringe plots at 100% load; (left to right) REF, CS, VSY**

In terms of shear stiffness, max. circumferential displacement was evaluated and plotted in Figure 13. At 100% load for example, torsional resistance of VSY design was only 10% less than that of REF design. CS design's shear compliance was however 64% higher than that of the referendum. The drastic shear stiffness reduction was expected to come from dominance of 0° and 90° in CS design.

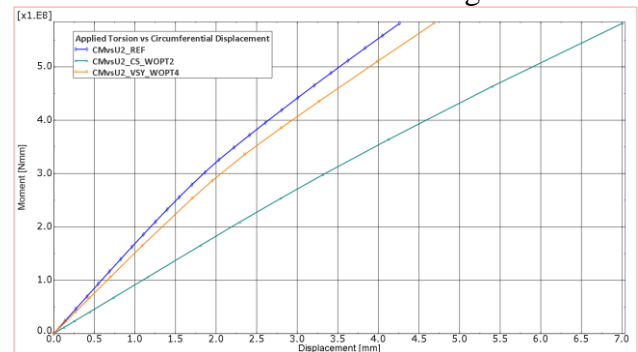


**Figure 13 Torsional moment VS Max. circumferential displacement plot**

	Reference Design	Constant-Stiffness Design		Variable-Stiffness Design	
			Improvement [%]		Improvement [%]
Eigen Buckling Factor [-]	0.500	0.355	-29	0.348	-30
1 <sup>st</sup> Buckling Mode					
Transverse Displacement Plot (Nonlinear)	0.52M <sub>max</sub>	0.36M <sub>max</sub>		0.28M <sub>max</sub>	

**Table 7 Linear VS Nonlinear buckling analysis**

Optimized for nonlinear buckling stability, critical bifurcation buckling load of CS and VSY designs were shown to be 30% lower than that of REF design as compared in Table 7. First buckling mode predicted by linear and nonlinear buckling analysis for each design is also illustrated and compared. Obviously, buckles around window were overlooked by the linear approach. It proved to be important that nonlinear buckling analysis was utilized in this optimization work.

## **6 Manufacturing Aspects**

For simplicity, manufacturing requirements, e.g. min. radius of fiber curvature, gaps/overlaps effects, were not yet included in this nonlinear buckling optimization work as structural improvements gained by ideal variable-stiffness panels was interested. Another reason was to observe on how far the current technological limitation, i.e. tow curvature, needed to be escalated in order to match the suggested optimal solution. Curvilinear-fiber laminates can be fabricated by several state-of-the-art automated technics. Two of them are proposed as potential methods for the optimal steered-fiber fuselage panel suggested in this paper:

### **6.1 Automated Fiber Placement (AFP)**

The most mature approach is currently the Automated Fiber Placement (AFP) machine where pre-impregnated fiber tows are steered on mold surface. The in-plane curvature of steered tows is however somewhat limited, hindering full design flexibility. The minimum allowable radius of 635mm was reported [21], while the optimal steered-fiber laminates found herein demanded as low as 326-mm radius. Clearly, a radical improvement in manufacturing process is needed if mechanical improvement offered by VSY design is to be fully realized. Another disadvantage of variable angle tow designs is inherited gaps and overlaps caused by shifted finite tow width [22]. As the curvature of the tow path increases, the area of tow gap or overlap increases. Tow overlap and tow drop technics can partially solve the problem.

### **6.2 Fiber Patch Preforming (FPP) [14]**

As mentioned in subsection 2.2, highly curved fiber pattern in circular fiber path around the window cutout may not be manufacturable by continuous carbon fibers. Instead, linearized circular fiber path can be achieved by automated Fiber Patch Preforming (FPP) technic where layers of repeatable, short fiber patches coated with adhesive are laid on component surfaces. The preforms are also compatible with any standard infiltration processes, including RTM. Due to fibers discontinuity, 14% reduction in fiber strengths were observed when optimal patch overlapping pattern was put into place. Young's moduli were proven to be unaffected by discontinuity nature. Material properties of circular fiber layers in this research were adjusted accordingly.

## **7 Conclusions**

In this paper, the shear post-buckling stability represented by max. transverse displacement was optimized through the use of steered-fiber laminates. The optimized curvilinear fiber panel increased post-buckling performance by 26% compared to a conventional reference design. Even though almost identical values were obtainable by optimal straight-fiber design, variable stiffness design showed 31% lower failure index at window cutout. The fact that mass saving potential can be fully realized only when buckling performance is improved and stress concentration is simultaneously mitigated to delay the first window frame's failure or debonding advocates the importance of stress-reducer laminates at the window frame.

Comparing linear eigen buckling analysis to nonlinear buckling analysis showed different first buckling modes. Bifurcation buckling analysis type was incapable of capturing buckles around weak window cutout. Geometrical nonlinearity consideration was necessary for buckling optimization of this particular fuselage panel.

Global Response Surface Method (GRSM) was employed as an optimization procedure. The response surface-based optimization was able to efficiently provide

global or close-to-global optimum in a highly nonconvex design optimization problem like this unconstrained variable-stiffness design optimization. The surrogate-modelling technic as well as optimization method deployed inside GRSM are however not fully described by Altair Engineering.

Future work will include compressive load as well as realistic combined shear-compression loads. Weight minimization instead of the presented buckling stability maximization is also planned. Strength and manufacturing constraints are to be included.

## 8 Contact Author Email Address

For further questions or contacts to the author, please mail to [ungwattanapanit@tum.de](mailto:ungwattanapanit@tum.de).

## References

- [1] IJsselmuiden T. Optimal Design of Variable Stiffness Composite Structures Using Lamination Parameters, Doctoral Thesis, *TU Delft*, Faculteit Luchtvaart -en Ruimtevaarttechniek, 2011.
- [2] Alhajahmad A, Design Tailoring of Panels for Pressure Pillowing Using Tow-Placed Steered Fibers, Doctoral Thesis, *TU Delft*, Faculteit Luchtvaart -en Ruimtevaarttechniek, 2008.
- [3] Lopes C, Gurdal Z and Camanho P, Variable-stiffness composite panels: Buckling and first-ply failure improvements over straight-fibre laminates, *Computer and Structures*, Vol. 86, pp 897-907, 2008.
- [4] Gürdal Z and Olmedo R. In-plane Response of Laminates with Spatially Varying Fiber Orientations: Variable Stiffness Concept, *AIAA Journal*, Vol. 31, No. 4, 1993.
- [5] van den Brink W, Vankan W and Maas R. Buckling-optimized variable stiffness laminates for a composite fuselage window section, *28<sup>th</sup> International Congress of The Aeronautical Sciences (ICAS 2012)*, Brisbane, Australia, 2012.
- [6] Degenhardt R, et al. Improved MATerial exploitation at safe design of COMposite airframe structures by accurate simulation of Collapse, *Composite Structures*, Vol. 73, pp. 175-178, 2006.
- [7] Nik M, Fayazbakhsh K, Pasini D and Lessard L. Surrogate-based multi objective optimization of a composite laminate with curvilinear fibers, *Composite Structures*, Vol. 94, pp 2306-2313, 2012.
- [8] Hyer M and Lee H. The use of curvilinear fiber format to improve buckling resistance of composite plates with central circular holes, *Composite Structures*, Vol. 18, pp 239–261, 1991.
- [9] Hyer M and Charette R. The use of curvilinear fiber format in composite structure design, *Proceedings of the 30th AIAA/ASME/ASCE/AHS/ASC Structures, Structural Dynamics and Materials (SDM) Conference*, New York, NY, USA, 1989.
- [10] Ungwattanapanit T and Baier H. Strength-stability optimization of hybrid-stiffness laminated plates with cut-outs subjected to multiple loads, *RAeS-3rd Aircraft Structural Design Conference*, Delft, Netherlands, 2012.
- [11] Ungwattanapanit T, Zhang Y and Baier H., Hybrid-stiffness laminated fuselage panels with window cutout optimized under strength and stability constraints, *17<sup>th</sup> International Conference on Composite Structures (ICCS17)*, Porto, Portugal, 2013.
- [12] Lynch C, Murphy A, Price M and Gibson A. The computational post buckling analysis of fuselage stiffened panels loaded in compression, *Thin-Walled Structures*, Vol. 42, pp 1445-1464, 2004.
- [13] Murphy A, Price M, Lynch C and Gibson A. The computational post-buckling analysis of fuselage stiffened panels loaded in shear, *Thin-Walled Structures*, Vol. 43, pp 1455-1474, 2005.
- [14] Meyer O. Kurzfaser-Preform-Technologie zur kraftflussgerechten Herstellung von Faserverbundbauteilen, Doctoral Thesis, *University of Stuttgart*, Institute of Aircraft Design, 2008.
- [15] Hexcel Composites. Prepreg Properties - HexPly® 8552 UD Carbon Prepregs – IM7, *Hexcel Composites*, Publication FTA 072e, February 2013.
- [16] Clarkson E. Hexcel 8552 IM7 unidirectional prepreg 190 gsm & 35% RC qualification statistical analysis report, *National Institute for Aviation Research*, Wichita State University, Report # NCP-RP-2009-028 Rev N/C, 2011.
- [17] Dassault Systèmes. Abaqus 6.13 Analysis User's Guide, *Dassault Systèmes*, April 2013.
- [18] Altair Engineering, Inc. HyperWorks 12.0 Desktop User Guides - HyperStudy, *Altair Engineering, Inc.*, 2013.
- [19] Pajot J. Optimal design exploration using Global Response Surface Method: Rail crush, HyperWorks, *Altair Engineering*, 2013.
- [20] Kocer F. One-click optimization, HyperWorks Insider, *Altair Engineering*, February 2014. (<http://insider.altairhyperworks.com/efficiently-produce-optimal-designs-make-decisions/>)
- [21] Nagendra S, Kodiyalam S, Davis J and Parthasarathy V. Optimization of Tow Fiber Paths for Composite Design, *Proceedings of the AIAA/ASME/ASCE/AHS/ASC 36th SDM Conference*, New Orleans, LA, pp 1031-1041, April 1995.
- [22] Gürdal Z and Tatting B. Tow-Placement Technology and Fabrication Issues for Laminated Composite Structures, *Proceedings of the AIAA/ASME/ASCE/AHS/ASC 46th SDM Conference*, Austin, TX, pp 2005-2017, April 2005.

### **Copyright Statement**

The authors confirm that they, and/or their company or organization, hold copyright on all of the original material included in this paper. The authors also confirm that they have obtained permission, from the copyright holder of any third party material included in this paper, to publish it as part of their paper. The authors confirm that they give permission, or have obtained permission from the copyright holder of this paper, for the publication and distribution of this paper as part of the ICAS 2014 proceedings or as individual off-prints from the proceedings.